International Journal of Mechanical Engineering and Applications
2019; 7(1): 1-7
http://www.sciencepublishinggroup.com/j/ijmea
doi: 10.11648/j.ijmea.20190701.11
ISSN: 2330-023X (Print); ISSN: 2330-0248 (Online)

Numerical Analyses on Liquid-Metal Magnetohydrodynamic Flow in 180°-Turn Channel

Hiroshige Kumamaru*, Naohisa Takagaki

Department of Mechanical Engineering, Graduate School of Engineering, University of Hyogo, Himeji, Japan

Email address:
h_kumamaru@ac.cyberhome.ne.jp (H. Kumamaru)

*Corresponding author

To cite this article:
Hiroshige Kumamaru, Naohisa Takagaki. Numerical Analyses on Liquid-Metal Magnetohydrodynamic Flow in 180°-Turn Channel. *International Journal of Mechanical Engineering and Applications*. Vol. 7, No. 1, 2019, pp. 1-7. doi: 10.11648/j.ijmea.20190701.11

Received: January 15, 2019; **Accepted**: February 19, 2019; **Published**: March 1, 2019

Abstract: Numerical calculations have been performed on liquid-metal magnetohydrodynamic (MHD) flow in a 180°-turn (i.e. hairpin-shaped) channel, in order to contribute to design of a fusion reactor blanket. A magnetic field is applied in a direction perpendicular to an inlet channel, a turning channel (turning section) and an outlet channel. The continuity equation, the momentum equation and the induction equation have been solved numerically. In this study, attention is focused on pressure drops along the channels and pressure distribution in the turning channel. The Hartmann number (indicating magnetic field strength), the Reynolds number and the channel aspect ratio, in the present calculations, cover 100 to 500, 1000 to 5000 and 1 to 1/4, respectively. The following things have become clear from calculation results. The total MHD pressure drop from a channel inlet to a channel outlet agrees approximately with that for the total channel length, meaning that the loss coefficient for the turning channel is nearly zero or small. For large Reynolds numbers, the pressure in the peripheral region of the turning channel becomes larger than that at the channel inlet, due to the centrifugal force acting in the turning channel. It is considered that this pressure increase should be taken into account in designing a fusion reactor blanket.

Keywords: Magnetohydrodynamic, MHD, Liquid Metal, U-Bend, 180°-Turn, Hairpin-Shaped

1. Introduction

In proposed blankets for fusion power plants to be realized in the future, liquid metals containing lithium are used as coolant while helium is also served as cooling material [1]. Liquid metals are excellent coolant having high heat capacity and thermal conductivity. However, when liquid metals flow in a strong magnetic field which confines reacting plasma in a fusion reactor core, there exists magnetohydrodynamic (MHD) interaction between the liquid-metal flow and the magnetic field, which generates a large MHD pressure drop. In order to decrease the MHD pressure drop, it is proposed that electrically-insulating flow channel inserts are used or electrical insulation coating of channel walls is applied.

Three-dimensional numerical calculations are indispensable in order to predict exactly liquid-metal MHD flows with changes in flow direction, channel cross section, applied magnetic field and others. In recent years, three-dimensional numerical calculations have been performed on MHD liquid-metal flows in magnetic field inlet-region or outlet-region [2-4], expanding channels [4-7], contracting channels [8, 9], U-bend channels [10], 180°-turn (hairpin-shaped) channels [11, 12], branching channels [13] and others.

Xiao et al. carried out numerical calculations on liquid-metal MHD flows in a 180°-turn (hairpin-shaped) square channel [11]. The channel walls were electrically-conducting, and the magnetic field was applied in the direction perpendicular to the plane of inlet and outlet channels.

Tassone et al. performed numerical calculations on liquid-metal MHD flows in a 180°-turn (hairpin-shaped) square channel in simulating a channel proposed by their blanket design [12]. The channel walls had non-uniform electrical conductivity, and the magnetic field was applied in the direction nearly perpendicular to the plane of inlet and outlet channels with inclination of 16° in simulating practical installation situation.

In this study, numerical calculations are performed on liquid-metal MHD flows in a 180°-turn (hairpin-shaped) square channel. The channel walls are assumed to be

electrically insulating (nonconducting), and the magnetic field is applied in the direction perpendicular to the plane of inlet and outlet channels. The *Ha* number and the *Re* number are changed from 100 to 500 and from 1000 to 5000, respectively. Also, the aspect ratio of the channel cross-section is varied from 1 to 1/4. In this study, attention is focused on pressure drops along the channels and pressure distribution in a turning channel (i.e. a turning section).

2. Numerical Calculations

2.1. Calculation Models

Figure 1 shows the calculation model. Considering symmetry in the z-direction, the calculations are performed only for 1/2 of the channel cross-section, i.e. from 0 to l_z. (The actual flow cross-section is from $-l_z$ to l_z.) The liquid metal flows into the inlet channel at x=0 in the range of $0<y<2l_y$. After passing through the inlet channel of $0<x<l_{x1}$, the liquid metal turns by 180° in the turning channel of $l_{x1}<x<l_{x2}$. Finally, after passing through the outlet channel of $l_{x1}>x>0$, the liquid metal flows out from the outlet channel at x=0 in the range of $2l_y<y<4l_y$.

The applied magnetic field is imposed in the z direction. The channel walls are assumed to be electrically insulating (nonconducting). The partitioning wall of $y=2l_y$ is treated as insulating wall with zero thickness in the present calculations.

2.2. Calculation Methods

Formulation based on induced magnetic field [14, 15] has been adopted in the present calculations. The continuity equation, the momentum equation and the induction equation are expressed respectively by:

$$\nabla \cdot \boldsymbol{v} = 0 \tag{1}$$

$$\rho\left[\frac{\partial \boldsymbol{v}}{\partial t} + (\boldsymbol{v}\cdot\nabla)\boldsymbol{v}\right] = -\nabla p + \eta\nabla^2\boldsymbol{v} + \frac{1}{\mu}(\nabla\times\boldsymbol{B})\times\boldsymbol{B_0} \tag{2}$$

$$\frac{\partial \boldsymbol{B}}{\partial t} = \nabla\times(\boldsymbol{v}\times\boldsymbol{B_0}) + \frac{1}{\sigma\mu}\nabla^2\boldsymbol{B} \tag{3}$$

Here, t, v, B, p and B_0 are the time, the velocity vector, the induced magnetic field vector, the pressure and the applied magnetic field vector, respectively, and ρ, η, μ and σ are the density, the viscosity, the magnetic permeability and the electric conductivity, respectively. The induced magnetic field (B) produced by the induced electric current is treated as an unknown variable together with the velocity (v) and the pressure (p). The third term in the right-hand side of (2) represents the Lorentz force. The induction equation, i.e. (3), is derived from Ohm's law, Faraday's law and Ampere's law in electromagnetism.

The basic equations are transformed into nondimensional expressions by introducing nondimensional variables and numbers presented below. The characteristic length is the half width of the channel in the direction of the applied magnetic field, i.e. l_z. The characteristic velocity is the average velocity in the x-direction, i.e. $\bar{u}$.

$$t^* = \frac{t}{l_z/\bar{u}},\ \boldsymbol{x}^* = \frac{\boldsymbol{x}}{l_z},\ \boldsymbol{v}^* = \frac{\boldsymbol{v}}{\bar{u}},\ p^* = \frac{p}{\rho\bar{u}^2},\ \boldsymbol{B}^* = \frac{\boldsymbol{B}}{\bar{u}\mu\sqrt{\sigma\eta}}, \tag{4}$$

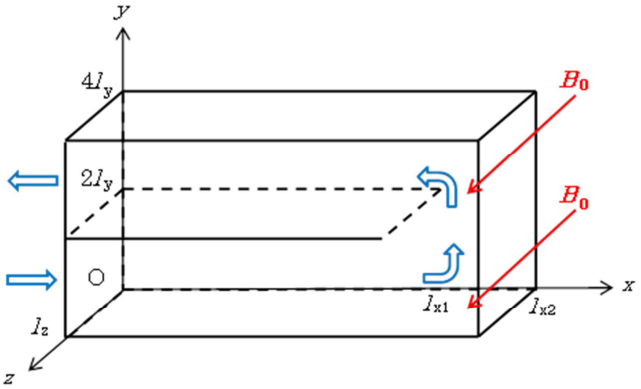

Note: The actual flow cross-section is from $-l_z$ to l_z.
$l_{x2} = l_{x1} + 2l_y$

Figure 1. *Calculation model.*

$$Re=\frac{\rho\bar{u}l_z}{\eta},\ Ha=B_0 l_z\sqrt{\frac{\sigma}{\eta}},\ Rm=\sigma\mu l_z\bar{u} \tag{5}$$

Here, Re, Ha and Rm are the Reynolds number, the Hartmann number and the magnetic Reynolds number, respectively. The final nondimensional basic equations are expressed by:

$$\nabla\cdot\boldsymbol{v} = 0 \tag{6}$$

$$\frac{\partial \boldsymbol{v}}{\partial t} + (\boldsymbol{v}\cdot\nabla)\boldsymbol{v} = -\nabla p + \frac{1}{Re}\nabla^2\boldsymbol{v} + \frac{1}{Re}(\nabla\times\boldsymbol{B})\times\boldsymbol{Ha} \tag{7}$$

$$\frac{\partial \boldsymbol{B}}{\partial t} = \frac{1}{Rm}\nabla\times(\boldsymbol{v}\times\boldsymbol{Ha}) + \frac{1}{Rm}\nabla^2\boldsymbol{B} \tag{8}$$

For simplification, star (*) is omitted in (6) through (8) and in the following description. Note that the Hartmann number Ha=(0, 0, Ha) is a vector with only known and constant z-component.

Regarding the boundary condition on the flow velocities, the inflow boundary condition is applied at the flow inlet, i.e. at x=0 in the range of $0<y<2l_y$, by giving the fully developed MHD flow velocity distribution. The outflow boundary condition is adopted at the flow outlet, i.e. at x=0 in the range of $2l_y<y<4l_y$, by giving the reference pressure.

Regarding the boundary condition on the induced magnetic fields, $\partial\boldsymbol{B}/\partial x = 0$ is applied at the flow inlet and the flow outlet. This means that the induced current does not change in the x-direction at the flow inlet and the flow outlet. Also, $\boldsymbol{B}$=0 is adopted at the walls by assuming that the walls are electrically insulating (nonconducting). The boundary conditions on the induced magnetic fields at the symmetry plane of z=0 are not intuitively clear. Thus, by calculating for the whole flow cross-section with small Re and Ha, it has been confirmed that the conditions are expressed by:

$$z = 0 : A(-z) = -A(z), B(-z) = -B(z), C(-z) = C(z)$$

where A, B and C are the x, y and z components of B, respectively. Note that A and B are odd functions of z though C is an even function of z.

The calculations are carried out using a grid of 60, 80 and 35 division in x, y and z directions, respectively, with gird elements closely spaced near the inlet and outlet of the turning channel. The discretization of the equations is performed with the finite difference method, and the MAC method is adopted as the solution procedure. The staggered-grid formation is used and the first-order accurate upwind differencing for the fluid convection terms in (7) is adopted.

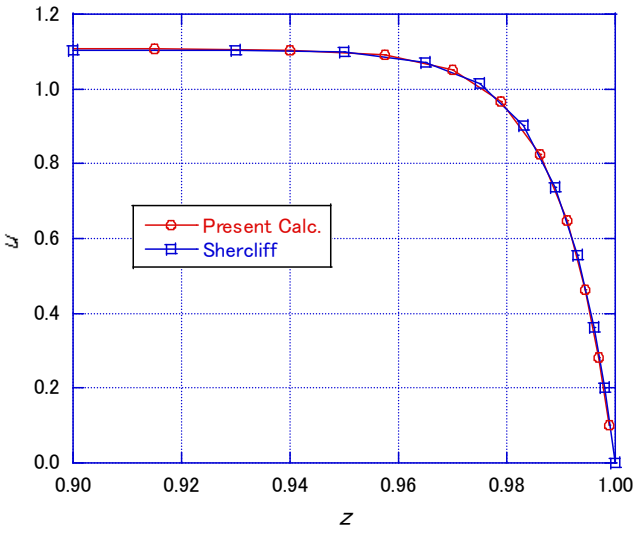

Figure 2. *Comparison of u(z) with Shercliff's solution.*

The calculations start from the initial conditions giving the fully developed velocity profile in the inlet and outlet channels, and an assumed velocity profile in the turning channel. The calculations continue until the velocity and the pressure distribution do not change.

3. Calculation Results

3.1. Verification and Validation

A base case calculation was carried out for Ha=100, Re=1000 and Rm=0.001. The aspect ratio (AR) of channel cross-section, i.e. l_y/l_z, is set to 1, thus l_y=1 and $2l_y$=2. The length l_{x1} is set to 10, thus l_{x2}(= l_{x1}+2l_y) becomes 12. Calculation results for a fully developed flow region in the inlet and outlet channels are compared with analytical solutions obtained by Shercliff [16, 17].

Figure 2 compares axial velocity (u) distribution along z-axis from z=0.9 to z=1.0 between the present calculation and the Shercliff analysis. (The distributions in the present calculation are the same between the inlet channel and the outlet channel.) The axial velocity distributions obtained in the present calculation agree well with that derived by Shercliff. Next, the pressure drops along the channel axes, $-\partial p/\partial x$, obtained in the present calculation are compared with that derived in Shercliff's analysis. The pressure drops in the present calculation, i.e. 0.112 in the inlet channel and 0.113 in the outlet channel, agree well with that in Shercliff's analytical solution, i.e. 0.111.

3.2. Base Case

The base case calculation was carried out for Ha=100, Re=1000, Rm=0.001 and AR=1, as mentioned in Sec. 3.1. These non-dimensional parameters simulate a liquid metal flow with an axial velocity of ~10 cm/s in a channel with ~1 cm width under an applied magnetic field of ~1 T.

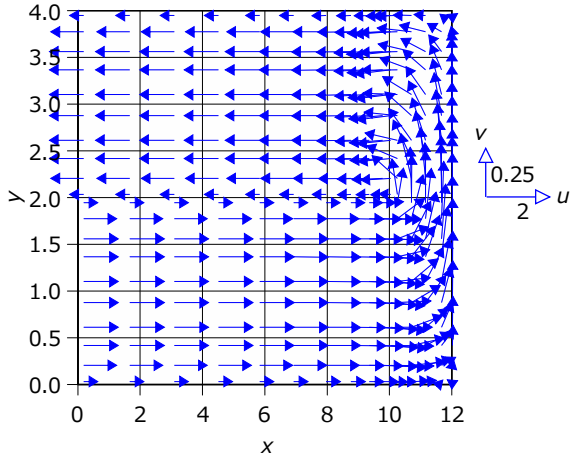

Figure 3. *Velocity (u, v) distribution in base case.*

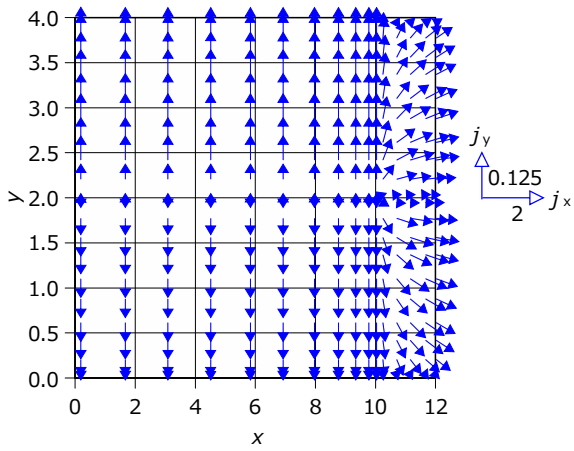

Figure 4. *Induced current (j_x, j_y) distribution in base case.*

Figure 3 shows the velocity vector (u, v) distribution in the x-y plane at z= 0. A velocity profile for fully-developed MHD flow appears in the inlet channel of 0<x<8 and in the outlet channel of 8>x>0. The flow turns by 180° relatively smoothly in the turning channel. A flow separation appears above the portioning wall at the entrance of the outlet channel (i.e. at x=10).

Figure 4 gives the induced electric current vector (j_x, j_y) distribution in the x-y plane at z= 0. The induced currents flow in the negative y-direction in the fully-developed flow region, i.e. 0<x<8, of the inlet channel. The induced currents run in the positive y-direction in the fully-developed flow region, i.e. 8>x>0, of the outlet channel. These induced

currents, which are uniform along the flow axis, produce uniform velocity profiles and constant MHD pressure drops along the flow axes in the fully-developed flow regions. In the turning channel, the induced currents flow outward in the directions nearly perpendicular to the flows. These induced currents also produce the MHD pressure drop; however, pressure changes produced by the centrifugal forces acting in the turning channel appear remarkably as mentioned below.

Figure 5 shows the pressure (p) contour map in the x-y plane at z= 0. Figure 6(a) gives the pressures along three lines, i.e. center line (red), inner line (blue) and outer line (green), explained in Figure 6(b). Due to the constant MHD pressure drop in the inlet and outlet channels, the pressure decreases linearly from the inlet (C_{in}, I_{in}, O_{in}) to the outlet (C_{out}, I_{out}, O_{out}) in the inlet and outlet channels. Since the centrifugal force acts in the turning channel, the pressure increase along the center line and the outer line and decreases along the inner line inside and near the turning channel. In particular, the pressure at the lower right, i.e. point O_1, becomes higher than that at the inlet, i.e. points C_{in}, I_{in}, O_{in}.

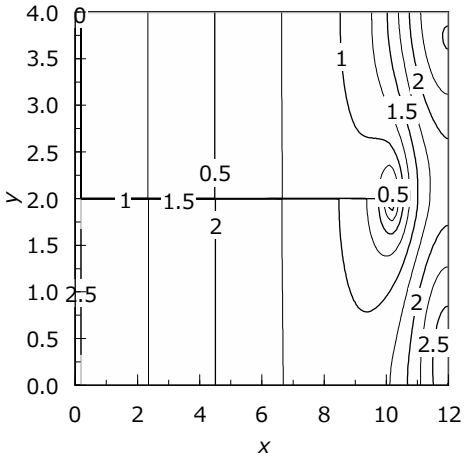

Figure 5. *Pressure (p) distribution in base case.*

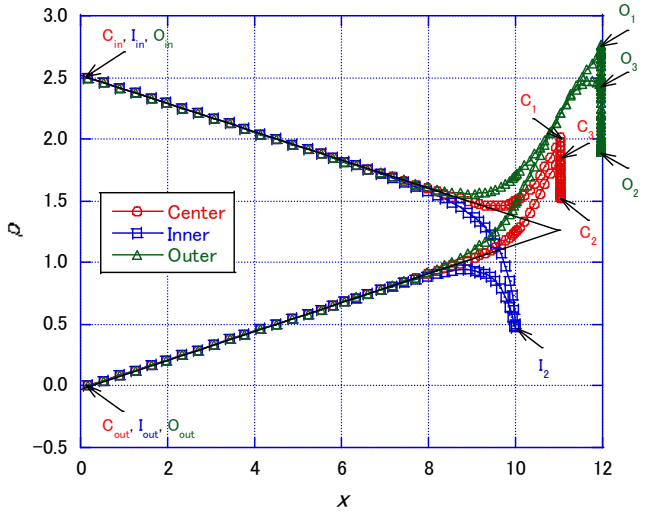

(a) For base case (Ha=100, Re=1000, AR=1).

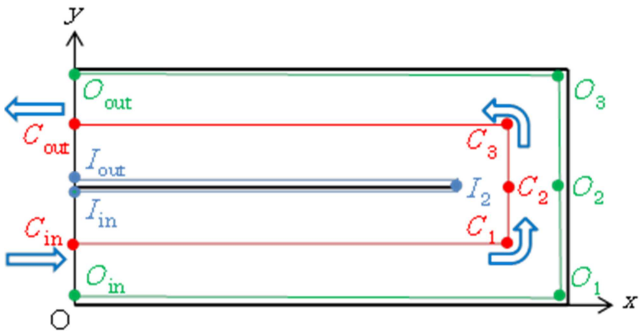

(b) Explanation of three lines.

Figure 6. *Pressures along three lines in base case.*

As indicated by black lines in Figure 6(a), extension lines of the pressure drops in the inlet channel and outlet channel intersect nearly at x=11 ($=l_{x1}+l_{x2}/2$). This means that the total pressure drop can be estimated by the pressure drop of the fully-developed flow through a channel with the total length of $22=2\times(l_{x1}+l_{x2}/2)$ and the loss coefficient for the turning channel is nearly zero. However, if the total length of the center line, i.e. $24=2\times(l_{x1}+l_{x2}/2)+2l_y$, is used, the loss coefficient becomes a minus small value, meaning that small pressure recovery occurs. Xiao et al. also presented a pressure drop change along inlet, turning and outlet channels giving pressure recovery in the turning channel [11]. It can be said from the above results that the loss coefficient for the turning channel is nearly zero or small. This statement is also true for calculation results presented in the following sections.

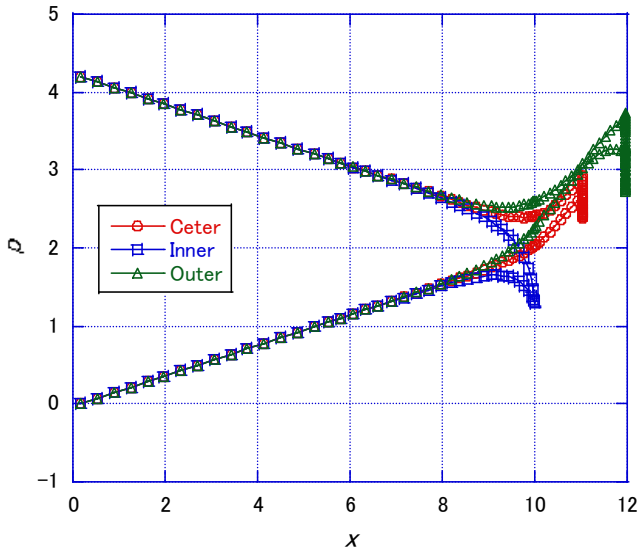

(a) Ha=200 (Re=1000, AR=1).

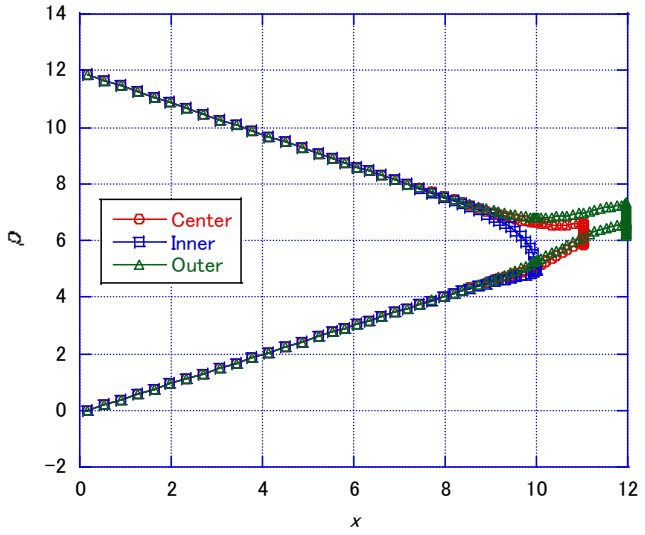

(b) Ha=500 (Re=1000, AR=1).

Figure 7. *Pressures along three lines, effects of Ha.*

3.3. Effect of Ha Number and Re Number

Numerical calculations were performed for the cases of *Ha*=200 and 500. The other parameters are the same as those for the base case. Figures 7(a) and 7(b) show the pressures along the three lines, i.e. center line (red), inner line (blue) and outer line (green), shown in Figure 6(b) for the cases of *Ha*=200 and 500, respectively. It can been seen by comparing Figure 6(a) (*Ha*=100), Figure 7(a) (*Ha*=200) and Figure 7(b) (*Ha*=500) that the higher the *Ha* number becomes, the larger the pressure drops in the inlet and outlet channels become. However, the pressure increase arising from the centrifugal force along the outer line in the turning tube is not remarkable for higher *Ha* number due to larger pressure drop along the flow axis.

Secondly, numerical calculations were carried out for the cases of *Re*=2000 and 5000. The other parameters are the same as those for the base case. Figures 8(a) and 8(b) show the pressures along the three lines for the cases of *Re*=2000 and 5000, respectively. Since the pressure was transferred into nondimensional one by $\rho\bar{u}^2$ (see (4)), the pressures in Figure 8(a) (*Re*=2000) and Figure 8(b) (*Re*=5000) should be multiplied by 4 and 25, respectively, in order to compare with the pressure in Figure 6(a) (*Re*=1000). The pressure increases caused by the centrifugal force along the outer and center lines in the turning tube become more remarkable for higher *Re* numbers. The pressures along the outer and center lines are considerably larger than that at the channel inlet. It is considered that this pressure increase should be taken into account in designing fusion reactor blankets.

Thirdly, numerical calculations were performed for the cases of *Ha*=200 & *Re*=2000 and *Ha*=500 & *Re*=5000. The other parameters are the same as those for the base case. Figures 9(a) and 9(b) show the pressures along the three lines for the cases of *Ha*=200 & *Re*=2000 and *Ha*=500 & *Re*=5000, respectively. As with the pressures in Figures 8(a) and 8(b), since the pressure was transferred into non-dimensional one by $\rho\bar{u}^2$ (see (4)), the pressures in Figure 9(a)

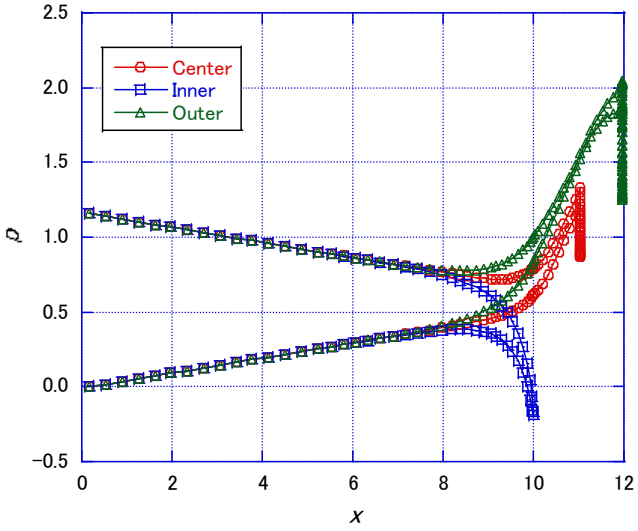

(a) Re=2000 (Ha=100, AR=1).

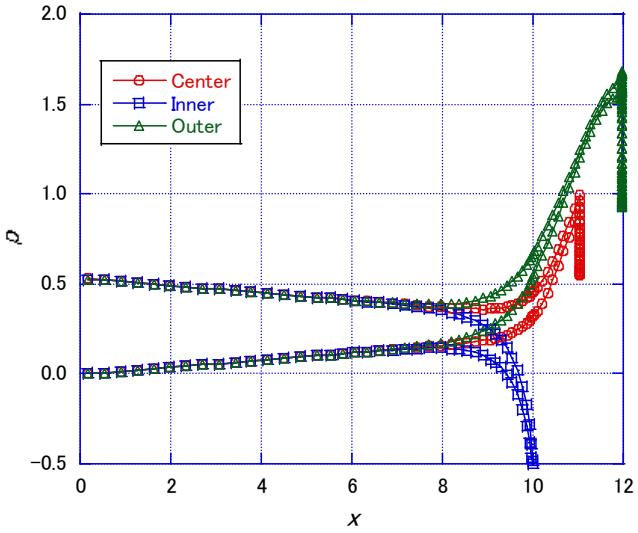

(b) Re=5000 (Ha=100, AR=1).

Figure 8. *Pressures along three lines, effects of Re.*

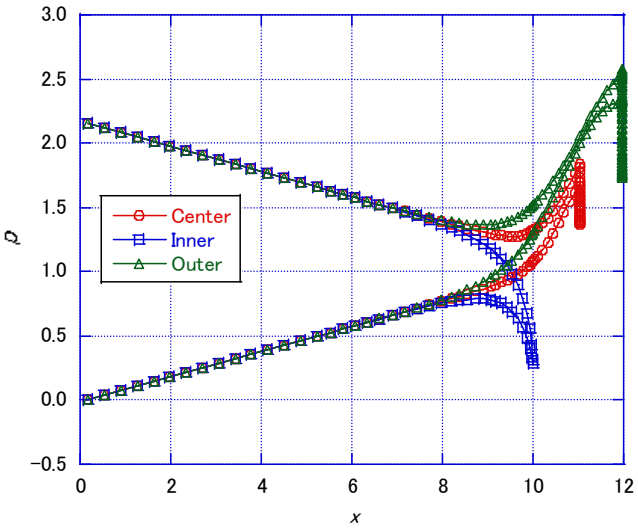

(a) Ha=200, Re=2000 (AR=1).

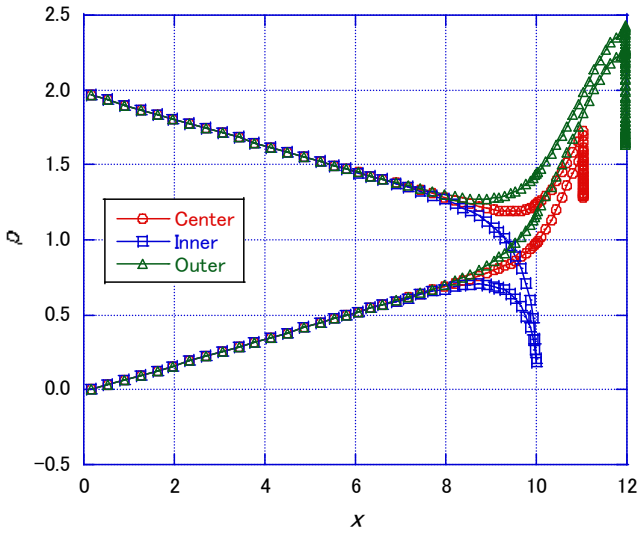

(b) Ha=500, Re=5000 (AR=1).

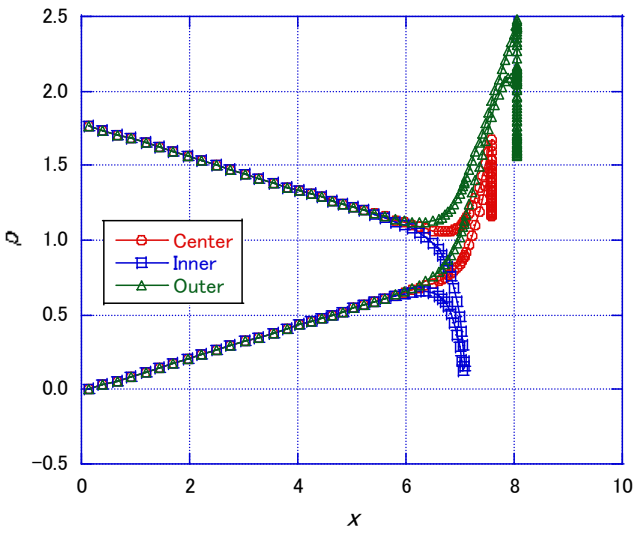

(a) AR=1/2 (Ha=$\sqrt{2}\times100$, Re=$\sqrt{2}\times1000$).

Figure 9. *Pressures along three lines, effects of Ha and Re.*

(*Re*=2000 & *Ha*=200) and Figure 9(b) (*Re*=5000 & *Ha*=500) should be multiplied by 4 and 25, respectively, in order to compare with the pressure in Figure 6(a) (*Re*=1000 & *Ha*=100). It can be seen that the pressure increase arising from the centrifugal force along the outer line in the turning tube becomes remarkable for higher *Re* numbers, even when the *Ha* number is large. The pressure along the outer line in the turning tube becomes larger than that at the channel inlet.

3.4. Effect of Aspect Ratio

Finally, numerical calculations were carried out for the cases of AR (aspect ratio) =1/2 and 1/4. The pressure drop along the flow channel becomes smaller for a smaller aspect ratio [16]. Figures 10(a) and 10(b) show the pressures along the three lines for the cases of AR=1/2 and 1/4, respectively. The calculations were performed in order to simulate channels with the same cross-section and the same length as for the base case. Since the characteristic length in transforming to nondimensional form is l_z (the half width of the channel in the direction of the applied magnetic field) (See (4)), the nondimensional channel lengths in Figure 10(a) (AR=1/2) and Figure 10(b) (AR=1/4) become $1/\sqrt{2}$ and 1/2 times those in Figure 6(a) (AR=1), respectively. (Also, both *Ha* and *Re* numbers in Figure 10(a) and Figure 10(b) become $\sqrt{2}$ and 2 times those in Figure 6(a), respectively.) However, since the average axial velocity ($\bar{u}$) is the same due to the same cross-section in dimensional (actual) geometry, the pressures in Figure 10(a) and Figure 10(b) can be compared directly with that in Figure 6(a). As expected, the pressure drops along the flow channels become smaller for smaller aspect ratios. The pressure increase caused by the centrifugal force along the outer line in the turning tube is significant even for smaller ARs. The pressure along the outer line in the turning tube becomes larger than that at the channel inlet.

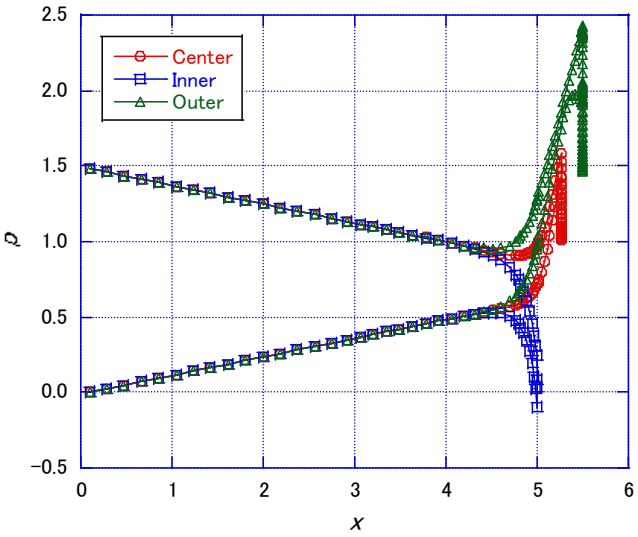

(b) AR=1/4 (Ha=200, Re=2000).

Figure 10. *Pressures along three lines, effects of AR.*

4. Conclusion

Numerical calculations have been performed on the liquid-metal MHD flow in the 180°-turn (i.e. hairpin-shaped) channel with nonconducting walls. The *Ha* number, the *Re* number and the channel aspect ratio cover 100 to 500, 1000 to 5000 and 1 to 1/4, respectively. The following conclusions have been obtained from the numerical calculations.

(1) The total MHD pressure drop through the inlet channel, the turning channel and the outlet channel agree approximately with that for the total channel length, i.e. the loss coefficient for the turning channel is nearly zero or small.

(2) For large *Re* numbers, the pressure in the peripheral region of the turning channel becomes large due to the centrifugal force, and the pressure becomes larger than that in the channel inlet. It is considered that this pressure increase should be taken into account in

designing fusion reactor blankets.

It is desirable to continue numerical calculations further in order to expand ranges of both the *Ha* number and the *Re* number up to ~10^4 and include 180°-turn channel with electrically-conducting walls.

References

[1] L. Buhler, C. Mistrangelo, J. Konys, R. Bhattacharyay, Q. Huang, D. Obukhov, S. Smolentsev, M. Utili, "Facilities, testing program and modeling needs for studying liquid metal magnetohydrodynamic flows in fusion blankets," Fusion Eng. Des., vol. 100, pp. 55-64, 2015.

[2] H. Kumamaru, K. Shimoda, K. Itoh, "Three-dimensional numerical calculations on liquid-metal magnetohydrodynamic flow through circular pipe in magnetic-field inlet-region," J. Nucl. Sci. Technol., vol. 44, pp. 714-722, 2007.

[3] H. Kumamaru, K. Itoh, Y. Shimogonya, "Three-dimensional numerical analyses on liquid-metal magnetohydrodynamic flow through circular pipe in magnetic-field outlet-region," InTechOpen, Trends in Electromagnetism -- From Fundamentals to Applications, Part 3, Chap. 9, pp. 207-222, 2012.

[4] T. Zhou, Z. Meng, H. Zhang, H. Chen, Y. Song, "Code validation for the magnetohydrodynamic flow at high Hartmann number based on unstructured grid," Fusion Eng. Des., vol. 88, pp. 2885-2890, 2013.

[5] C. N. Kim, "Liquid metal magnetohydrodynamic flows in an electrically conducting rectangular duct with sudden expansion," Computers & Fluids, vol. 89, pp. 232-241, 2014.

[6] J. Feng, Q. He, H. Chen, M. Ye, "Numerical investigation of magnetohydrodynamic flow through sudden expansion pipes in liquid metal blankets," Fusion Eng. Des., vol. 109-111, pp. 1360-1364, 2016.

[7] H. Kumamaru, "Numerical analyses on liquid-metal magnetohydrodynamic flow in sudden channel expansion," J. Nucl. Sci. Technol., vol. 54, pp. 242-252, 2017.

[8] C. N. Kim, "A liquid metal magnetohydrodynamic duct flow with sudden contraction in a direction perpendicular to a magnetic field," Computers & Fluids, vol. 108, pp. 156-167, 2015.

[9] H. Kumamaru, "Numerical analyses on liquid-metal magnetohydrodynamic flow in sudden channel contraction," J. Nucl. Sci. Technol., vol. 54, pp. 1300-1309, 2017.

[10] Q. He, J. Feng, H. Chen, "Numerical analysis and optimization of 3D magnetohydrodynamic flows in rectangular U-bend," Fusion Eng. Des., vol. 109-111, pp. 1313-1317, 2016.

[11] X. Xiao, C. N. Kim, "Magnetohydrodynamic flows in a hairpin duct under a magnetic field applied perpendicular to the plane of flow," Appl. Math. Comput., vol. 240, pp. 1-15, 2014.

[12] A. Tassone, G. Caruso, A. D. Nevo, I. D. Piazza, "CFD simulation of the magnetohydrodynamic flow inside the WCLL breeding blanket module," Fusion Eng. Des., vol. 124, pp. 705-709, 2017.

[13] C. Mistrangelo, L. Buhler, "Liquid metal magneto-hydrodynamic flows in manifolds of dual coolant lead lithium blankets," Fusion Eng. Des., vol. 89, pp. 1319-1323, 2014.

[14] A. Patel, R. Bhattacharyay, R. Srinivasan, E. Rajendrakumar, P. Bhuyan, P. Satyamurthy, P. Swain, K. S. Goswami, "3D thermo-fluid MHD simulation of single straight channel flow in LLCB TBM," Fusion Eng. Des., vol. 87, pp. 498-502, 2012.

[15] C. Kawczynski, S. Smolentsev, M. Abdou, "An induction-based magnetohydrodynamic 3D code for finite magnetic Reynolds number liquid-metal flows in fusion blankets," Fusion Eng. Des., vol. 109-111, pp. 422-425, 2016.

[16] J. A. Shercliff, "Steady motion of conducting fluids in pipes under transverse magnetic fields," Proc. Camb. Phil. Soc., vol. 49, pp. 136-144, 1953.

[17] S. Smolentsev et al., "An approach to verification and validation of MHD codes for fusion applications," Fusion Eng. Des., vol. 100, pp. 65-72, 2015.